A Single-Particle Char Gasification Model

A model is developed for the gasification of a single-char particle in an environment of water, hydrogen, carbon dioxide, carbon monoxide and methane, existing in the gasification zone of a reactor. The model, consisting of the mass and energy conservation equations, together with the Stefan-Maxwell relations includes the intraparticle effects and the change in internal surface area. It is found that the intraparticle effects and the surface area effects are significant and hence cannot be neglected, and the situation becomes more acute with increasing particle size and high temperatures. Comparisons with other models and existing empirical relations show that the model agrees well when diffusional effects are minimal, but at higher temperature and large particle size there is a significant difference. The model may be used to discriminate among various idealized models such as the homogeneous and the shrinking core model. The convective terms in the Stefan-Maxwell relations have negligible influence. The analysis can be directly used in the modeling studies of gasification reactors and will be so applied in a later paper.

B. SRINIVAS

and

NEAL R. AMUNDSON

University of Houston
Houston, Texas 77004

SCOPE

It is well known that one of the processes in the conversion of the vast reserves of coal to clean fuel is coal gasification using fluidized bed reactors. Coal and coal char can react with steam, hydrogen and carbon dioxide to give gaseous products which can be used as fuel. The heat required by this process may be supplied by combustion of part of the coal. When steam and oxygen are fed into a fluidized bed reactor, it has been shown (Caram and Amundson, 1979) that carbon combustion occurs in a very shallow portion of the bed, and hence a major portion of the reactor is the gasification zone. There is extensive literature on coal/char combustion, but the gasification process has received less attention. In modeling of gasification reactors, researchers either use empirical chemical kinetics such as that of Johnson (1974) or Gibson and Euker (1975), or use simplified kinetics and assume uniform reaction throughout the particle, neglecting the transport effects. Most mathematical analyses have been limited to a single reaction. Application of such analyses to more complicated systems where many simultaneous reactions take place is not simple. It is known that different kinds of coal char may have a wide range of reactivity, one reason being the different internal pore structure and available surface for reaction. Furthermore, the structure and the available surface change significantly during the gasification process. Since these factors vary widely with different coal chars, the application of empirical kinetics, determined for a few coal chars under restricted experimental conditions, to more complex and diverse processes is questionable. Moreover, the assumption of uniform reaction within the particle is not always justified. The purpose of this work is to develop a coupled transport and reaction model to determine the effects of various parameters such as ambient temperature, ambient concentration of reactant species, system pressures, particle size, etc.

The model developed consists of the mass and energy balance equations together with the Stefan-Maxwell relations. Intraparticle diffusion and structural changes of the particle during gasification are included. The char particle, composed of fixed carbon and ash, being gasified in an environment of water, carbon dioxide, carbon monoxide and methane can be described by four reactions, namely, steam gasification, carbon dioxide gasification, hydrogasification and the water-gas shift reaction. The non-Stefan flow problem is solved for various parametric conditions, and the Stefan-flow problem is solved to bring out the differences between the two. Finite difference and orthogonal collocation techniques are used to solve the system of differential equations.

CONCLUSIONS AND SIGNIFICANCE

The concentration profiles show an unusual behavior with respect to carbon dioxide as a consequence of a complex interaction between the shift reaction with the other reactions. Under some ambient conditions, large concentration gradients give rise to strong conversion profiles and in some cases shrink the core to a certain extent.

A parametric study shows that the gain due to increase in system pressure diminishes at higher values of the pressure. Diffusional resistance is more significant at higher temperatures and worsens with increase in particle size. Furthermore, the gas film resistance can be important under some conditions. At lower ambient temperatures, though carbon dioxide gasification is taking place, the net result is production of carbon dioxide. The situation, reversing at higher temperatures, results in net consumption of carbon dioxide, and carbon monoxide is the major product. An increase in ambient steam concentration is advantageous, whereas an increase in hydrogen concentration is disadvantageous with respect to gasification rates. Comparisons with the results obtained from Johnson's relations show that diffusional effects are significant and may not be neglected. The convective terms in the system of equations do not change the behavior of the system to a great extent and may be neglected in reactor modeling studies.

0001-1541-80-3616-0487-$01.25.

INTERNAL STRUCTURE AND KINETICS

The rates of gasification depend on the nature and origin of the char. In addition, the reactivity and pore structure depend greatly on the history of its formation, such as, temperature of pretreatment, rate of heating, its environment during pretreatment and many others. Most of the surface area is provided by the micropores and a small fraction by the macropores. There have been some studies on the change of pore characteristics and available surface area with gasification (Kawahata and Walker, 1963; Turkdogen et al., 1970; Walker et al., 1953; Petersen et al., 1955; Hashimoto and Silveston, 1973*a,b*, Dutta et al., 1977). In almost all cases, it was found that the surface area initially increased with gasification and then dropped sharply at higher conversions. The increase in the surface area is due to the formation of new pores by preferential removal of carbon atoms or opening of new pores which existed originally but were closed and the enlargement of pores which existed or were newly opened. At the same time, there is a decrease in surface area due to the collapse of two pores by gasification of the pore wall. The increase in surface area dominates at low carbon conversions, and the death rate dominates at higher conversions. However, a situation where there is only a loss of surface area is possible. For this study, the correlation for relative available surface area given by Dutta et al. (1977) is used

$$a = 1 \pm 100\, X^{\nu\gamma}\, e^{\gamma X} \tag{1}$$

The relative available pore surface area is defined as the ratio of the available specific pore surface area at any stage of conversion to the specific pore surface area at zero conversion.

In the literature, one can find many investigations on the gasification reactions. The reader is directed to several reviews available: Walker et al. (1959), Mulcahy and Smith (1969), Field et al. (1967) and Fredersdorff and Elliott (1963). Unfortunately, kinetics of these reactions appear in various forms, and only a few are based on the actual surface area available for reaction. In many cases, the form of carbon used is graphite, and the results may not be applicable to reactions with coal/char due to basic structural difference. As there are many discrepancies in the data, we should treat the rate constants as parameters.

Steam Gasification: $C + H_2O \rightarrow CO + H_2$ (endothermic, heterogeneous)

For this reaction, Hedden and Lowe (1967) present kinetics which are most useful to us. Since the rates were determined using graphite, we can expect them to be higher for coal/char. The rate is given by

$$rs_1 = \frac{k_1 C_1}{1 + k_{12} C_2} \quad \text{(kgmole } H_2O/m^2\text{-s)}$$

For this study we will assume

$$k_1 = 3.85\times10^7 \exp(-284\,702.4/RT)\, m^3/m^2\left(\begin{matrix}\text{internal}\\ \text{surface area}\end{matrix}\right)\text{-s}$$

$$k_{12} = 95.7 \exp(60\,708.6/RT)\ m^3/\text{kgmole}$$

Carbon Dioxide gasification: $C + CO_2 \rightarrow 2CO$ (endothermic, heterogeneous)

The rate of the carbon-carbon dioxide reaction has been studied by various investigators (see, Hedden and Lowe, 1967; Yang and Steinberg, 1977; Dutta et al., 1977). The data show considerable discrepancy in activation energies, ranging from 45 to 90 kcal/mole. Some instances of carbon monoxide inhibition, at low pressure, have been reported. We will, however, for this study choose the rate expression given by Dutta et al. (1977):

$$rs_2 = k_2 C_4 \quad \text{(kgmole } CO_2/\text{s-m}^2\text{)}$$

where

$k_2 = 370 \exp(-248\,109.8/RT)\, m^3/\text{s-m}^2$ (internal surface area)

Hydrogasification: $C + 2H_2 \rightarrow CH_4$ (exothermic, heterogeneous)

Blackwood (1959) measured hydrogasification rates, up to 40 atm, for coconut chars (~50 m^2/g) and presented

$$r_{s3} = k_3 p_{H_2} \text{ (kg mole } CH_4/m^2\text{-s)}$$

where $k_3 = 5.82 \times 10^{-11} \exp(-149\,050.1/RT)$ kg mole/s-(N/m^2)-m^2 (internal surface area)

Water gas shift reaction: $CO + H_2O \rightarrow CO_2 + H_2$ (homogeneous, exothermic)

In almost all cases, this reaction is considered to be in equilibrium. The equilibrium constant is given by

$$\text{Log}_{10} K = -1.6945 + 1\,855.6/T$$

(Fredersdorff and Elliott, 1963)

The heterogeneous reaction rates are based on unit internal surface area. Converting them to unit volume of the particle, for the j^{th} reaction, we have

$$r_j = rs_j \cdot S \cdot a \cdot \rho_0 (1 - X_r) \cdot W_b \quad \text{kg mole/m}^3\text{-s}, \quad j = 1,2,3$$

Thus, the reaction rates are a function of both carbon conversion and the available pore surface area.

THE MODEL

We will consider a spherical char particle surrounded by a gas film to be gasified in a fixed environment consisting of water, carbon dioxide, carbon monoxide, hydrogen and methane. This is a typical situation in the gasification zone of a fluidized bed or a moving bed reactor. Since the concentrations of the species and the temperature in the environment are known, we will assume that the following reactions take place:

1. $C + H_2O \rightarrow CO + H_2$
2. $C + CO_2 \rightarrow 2CO$
3. $C + 2H_2 \rightarrow CH_4$
4. $CO + H_2O \rightleftarrows CO_2 + H_2$

The heterogeneous reactions (1, 2 and 3) take place within the particle, and the homogeneous reaction (4) occurs everywhere. The gas film around the particle is characterized by the mass transfer coefficients; we will assume that it is the same for all species. The binary diffusion coefficient $\mathscr{D}_{ij}$ for the ij^{th} pair is assumed to be the same for all the species ($\mathscr{D}=\mathscr{D}_{ij}$) except hydrogen. Since the diffusivity of hydrogen is very high, it is assumed to be infinite. The effective diffusivity inside the particle is taken as $D = \epsilon^2\mathscr{D}$. We will assume that there is no temperature gradient within the particle owing to the large thermal conductivity of the solid. However, the temperature difference between the particle and the bulk is considered. We will follow the changes occurring in the particle during gasification. Initially, there is no ash layer around the particle, and, further, any ash layer formed during the course of gasification does not peel off. Thus, the size of the particle remains constant. We will assume that the pseudo steady state analysis is valid; that is, at any instant the particle looks as if it is at steady state. Also, constant physical properties will be assumed throughout the analysis.

Mass balance—gaseous species

The mass balance for the i^{th} species within the particle at steady state is given by

$$-\nabla N_i + \sum_{j=1}^{4} \alpha_{ij} r_j = 0 \quad \forall i \neq 2 \tag{2}$$

together with the boundary conditions

$$N_i = -k_g \cdot C(x_{bi} - x_i) \quad \text{at } r = R_c \tag{3a}$$

$$N_i = 0 \quad \text{at } r = 0 \tag{3b}$$

where N_i is characterized by the Stefan-Maxwell relation

$$\nabla x_i = \sum_{k=1}^{5} \frac{1}{C\,\mathcal{D}_{ik}} (x_i N_k - x_k N_i) \tag{4}$$

If we include the assumption regarding diffusion coefficients, Equation (4) reduces to

$$N_i = -CD\nabla x_i + x_i \sum_{k=1}^{5} N_k \nabla_i \neq 2 \tag{5a}$$

and,

$$\nabla x_2 = 0 \tag{5b}$$

Equations (5*b*) and (3*a*) give

$$x_2 = x_{b2} \tag{6}$$

At any point in the system, the following stoichiometric relations hold:

$$N_2 = -N_1 - 2N_5 \tag{7a}$$

and

$$N_3 = -N_1 - 2N_4 \tag{7b}$$

Hence

$$\sum_{i=1}^{5} N_i = -(N_1 + N_4 + N_5) \tag{8}$$

From (5*a*) and (8), we obtain

$$(N_1 + N_4 + N_5) = \frac{-CD\nabla(x_1+x_4+x_5)}{(1+x_1+x_4+x_5)} \tag{9}$$

From (2), we have

$$-\nabla N_1 - r_1 - r_4 = 0 \tag{10a}$$

$$-\nabla N_3 + r_1 + 2r_2 - r_4 = 0 \tag{10b}$$

$$-\nabla N_4 + r_4 - r_2 = 0 \tag{10c}$$

$$-\nabla N_5 + r_3 = 0 \tag{10d}$$

Since the relation, $\sum_i x_i = 1$ must be satisfied everywhere, the set of Equations (10*a*), (10*b*) and (10*c*) is dependent. Also, the shift reaction is at equilibrium; by eliminating r_4, the loss of an equation is compensated for by the equilibrium condition. After manipulating the equations for easier mathematical handling, we obtain

$$-\nabla(N_1 + N_4 + N_5) - r_1 + r_2 + r_3 = 0 \tag{11a}$$

$$-\nabla(N_5) + r_3 = 0 \tag{11b}$$

$$x_4 x_2 / x_3 x_1 = K \tag{11c}$$

$$\sum_i x_i = 1 \tag{11d}$$

If we use Equations (5*a*) and (9), the above equations become

$$CD\,\nabla\left\{\frac{x_5\nabla(x_1+x_4+x_5)}{(1+x_1+x_4+x_5)}\right\} - r_1 - r_2 + r_3 = 0 \tag{12a}$$

$$CD\left\{\nabla^2 x_5 - \nabla\left(\frac{x_5\nabla(x_1+x_4+x_5)}{(1+x_1+x_4+x_5)}\right)\right\} + r_3 = 0 \tag{12b}$$

$$x_4 x_2 / x_3 x_1 = K \tag{12c}$$

$$\sum_i x_i = 1 \tag{12d}$$

where

$$\nabla^2 \equiv \frac{1}{r^2}\frac{d}{dr}\left(r^2\frac{d}{dr}\right)$$

and ∇ takes the appropriate form depending on the places it occurs in the equation.

The boundary conditions (3*a*) and (3*b*) become

$$\frac{\nabla(x_1+x_4+x_5)}{(1+x_1+x_4+x_5)} = \frac{k_g}{D}(x_{b1}+x_{b4}+x_{b5}-x_1-x_4-x_5) \quad \text{at } r=R_c \tag{13a}$$

$$\nabla x_5 - x_5\frac{\nabla(x_1+x_4+x_5)}{(1+x_1+x_4+x_5)} = \frac{k_g}{D}(x_{b5}-x_5) \quad \text{at } r=R_c \tag{13b}$$

$$\frac{dx_i}{dr} = 0 \quad \text{at } r = 0 \quad \forall i \neq 2 \tag{13c}$$

Nondimensionalizing (12) and (13), we have†

$$\nabla^*\left[\frac{\nabla^* z}{1+z}\right] - \beta(r_1+r_2-r_3) = 0 \tag{14a}$$

$$\nabla^{*2} x_5 - \nabla^*\left(x_5\frac{\nabla^* z}{1+z}\right) + \beta r_3 = 0 \tag{14b}$$

$$x_4 x_2 / x_3 x_1 = K \tag{14c}$$

$$\sum_i x_i = 1 \tag{14d}$$

and

$$\left.\begin{aligned} \frac{\nabla^* z}{(1+z)} &= \frac{Sh}{2}(z_b - z) \\ \nabla^* x_5 - x_5\left(\frac{\nabla^* z}{1+z}\right) &= \frac{Sh}{2}(x_{b5}-x_5) \end{aligned}\right\} \text{at } \xi = 1 \tag{15a}$$

$$\frac{dx_i}{d\xi} = 0 \quad \text{at } \xi = 0 \tag{15b}$$

where

$$\left.\begin{aligned} &\nabla^{*2} \equiv \frac{1}{\xi^2}\frac{d}{d\xi}\left(\xi^2\frac{d}{d\xi}\right) \\ &\nabla^* \equiv \frac{d}{d\xi}; \quad \beta = \frac{R_c^2}{CD} \\ &z = x_1 + x_4 + x_5 \text{ and } z_b = x_{b1} + x_{b4} + x_{b5} \end{aligned}\right\} \tag{15c}$$

Carbon balance

The consumption of carbon is given by

$$\frac{d\rho}{dt} = -12(r_1+r_2+r_3) \quad (\text{kg/m}^3\text{-s}) \tag{16}$$

We define carbon conversion as the ratio of the amount of carbon gasified to the original amount of carbon. At any point within the particle

$$X_r = \frac{12}{\rho_0 W_b}\int_0^t (r_1 + r_2 + r_3)dt \tag{17}$$

and the average conversion of the particle

$$X = \frac{12}{M_0 W_b}\int_0^t \left(\int_V (r_1+r_2+r_3)dV\right)dt \tag{18}$$

Energy balance

Formulating the energy balance at the surface of the particle, we obtain

$$\frac{d}{dt}\left(\frac{M}{12}C_{ps}T_p\right) = h.A.\,(T_b - T_p) - A\sum_i N_i\tilde{h}_i \tag{19a}$$

with initial conditions

$$T_p = T_b \text{ and } M = M_0 \tag{19b}$$

where

$$\tilde{h}_i = \tilde{h}_i^\circ + C_{pi}\Delta T \tag{19c}$$

† Note, ∇^* can either be $d\cdot/d\xi$ or $1/\xi^2\, d/d\xi\,(\xi^2\cdot)$, depending on its function.

The above sets of Equations (14), (15), (16), (17), (18) and (19) are to be solved for, x_1, x_3, x_4, x_5, X_r, X, and T.

Effectiveness factors

We will define effectiveness factors in two different ways:

1. The effectiveness factor (EF) is defined as the ratio of the observed total reaction rate at any instant to the total reaction rate at that instant if the concentrations of the reactants were equal to their bulk values everywhere and at the bulk temperature; that is

$$\mathrm{EF} = \frac{\int_V (r_1+r_2+r_3)dV}{V_p(r_1+r_2+r_3)|_{T_b,x_{bi}}} \tag{20a}$$

2. The effectiveness factor (EF2) is defined as the ratio of the observed total reaction rate at any instant to the total reaction rate at time $t = 0$, if the concentrations of the reactant were equal to their bulk values everywhere and at the bulk temperature; that is

$$\mathrm{EF2} = \frac{\int_V (r_1+r_2+r_3)dV}{V_p(r_1+r_2+r_3)|_{T_b,x_{bi},a=1}} \tag{20b}$$

NON-STEFAN FLOW PROBLEM

Expecting the convective terms to be insignificant, for simplicity and as a first approximation, we will neglect the convective terms. Then, the Stefan-Maxwell equation reduces to

$$N_i = -CD\nabla x_i \tag{21}$$

With this, the conservation Equations (14) reduce to

$$\nabla^{*2}(x_1 + x_4) - \beta(r_1 + r_2) = 0 \tag{22a}$$

$$\nabla^{*2} x_5 + \beta(r_3) = 0 \tag{22b}$$

$$x_4x_2/x_3x_1 = K \tag{22c}$$

$$\sum_i x_i = 1 \tag{22d}$$

and the boundary conditions (15) reduce to

$$\frac{dx_i}{d\xi} = \frac{Sh}{2}(x_{bi} - x_i) \quad \forall i \neq 2 \quad \text{at } \xi = 1 \tag{23a}$$

$$\frac{dx_i}{d\xi} = 0 \quad \forall_i \neq 2 \text{ at } \xi = 0 \tag{23b}$$

This above set is to be solved together with the carbon and energy balance equations.

Solution

1. Non-Stefan flow problem: no analytical solution is possible for the sets of Equations (22) and (23) together with the carbon and energy balance equations. A finite difference numerical scheme was devised, but for these sets of equations the scheme was unstable. Hence, the equations are transformed using the transformation

$$y_i = x_i\xi \tag{24}$$

At time $t = 0$ (zero conversion), since x_2 is known everywhere, (22b) has an analytic solution. This, however, is not true for conversions greater than zero. Thus, with x_5 known everywhere, it is required to determine y_1, y_4 and y_3. The assumption of a value for y_1 at $\xi = 1$, fixes y_4 and y_3 at $\xi = 1$ by conditions (22c) and (22d). Once the values at the external boundary are known, marching towards the center, y_i's at the interior node point are determined from the differential equation and the boundary condition at $\xi = 1$, cast in the difference form. This procedure is repeated with new values of y_1 till the boundary condition at the center is satisfied. It was necessary to divide the region into 100 parts. In the time space, the profiles at $t_{k-1}$are used as the guess values for time t_k. Δt of 1 to 4 s was found adequate, and the convergence for subsequent time intervals was quite fast. This procedure is continued till 99% of the carbon in the particle is consumed.

2. Stefan-flow problem: the solution of the sets of Equations (14), (15), (17), (18) and (19) is unstable, and no convergence is obtained. It is necessary to transform the equation to a simpler form. We define

$$\overline{w} = [\ln(1+z)]\xi \tag{25}$$

and the equations reduce to

$$\frac{d^2\overline{w}}{d\xi^2} - \beta\xi(r_1 + r_2 + r_3) = 0 \tag{26a}$$

$$\frac{d^2y_5}{d\xi^2} - \left(\frac{dy_5}{d\xi} - \frac{y_5}{\xi}\right)\left(\frac{d\overline{w}}{d\xi} - \frac{\overline{w}}{\xi}\right)\frac{1}{\xi} + y_5\beta(r_3 - r_1 - r_2) + \beta\xi r_3 = 0 \tag{26b}$$

$$y_4y_2/y_3y_1 = \mathrm{K} \tag{26c}$$

$$\sum_i y_i = \xi \tag{26d}$$

boundary conditions

$$\left.\begin{aligned} \frac{d\overline{w}}{d\xi} &= \overline{w} + \frac{Sh}{2}(z_b - z) && (27a)\\ \frac{dy_5}{d\xi} &= y_5 + y_5\,\frac{Sh}{2}(z_b - z) + \frac{Sh}{2}(x_{b5} - y_5) && (27b) \end{aligned}\right\} \text{ at } \xi = 1$$

and

$$\overline{w} = 0\ ;\ y_5 = 0 \quad \text{at } \xi = 0 \tag{27c}$$

For the finite difference scheme, we need to guess molefractions of two species at the external boundary. The assumption of values for y_1 and y_5 determines y_3 and y_4 and hence, $\overline{w}$. $\overline{w}$ and y_5 at the subsequent node points are determined using (26a), (27a) and (27b), respectively. The rest of the procedure is as given for the non-Stefan flow problem. In some cases, orthogonal collocation technique (Villadsen and Michelsen, 1978) was used and in general was found superior to the finite difference scheme. When the concentration profiles become very steep, either spline collocation or a stretching transformation was used.

All calculations, unless otherwise mentioned, are done for IGT char 155 (Dutta et al., 1977). Char data and the physical properties used in the computations are listed in Table 1.

RESULTS AND DISCUSSION

We will analyze the non-Stefan flow problem (that is, simplified problem) and present the results in most cases, but later some calculations of the Stefan-flow problem (complete problem) will be discussed. Before we proceed, certain points should be clarified. In our model we have assumed zero temperature gradient within the particle. The thermal conductivity of coal increases rapidly above 1 000°K and further; the thermal conductivity of char particles is higher than that of coal particles (Badzioch et al., 1964). The maximum temperature difference within the particle can be estimated by considering the temperature equation along with the mass balance equations and obtaining temperature in terms of the molefractions of the species. With the constraints that $\Sigma x_i = 1$ and the equilibrium condition, a set of molefractions to give maximum temperature difference is chosen. Such an analysis gave the maximum temperature difference to be not greater than 3.5°K. For a fixed pressure and temperature, only the molefractions of three out of the five species present in the ambient are independent; the water-gas shift equilibrium forces the dependency. Figures 1 *a*, *b*, *c* and *d* represent the concentration profiles within the particle for various ambient temperatures and external film resistance. The steam molefraction is seen decreasing towards the center in all cases, and the main product carbon monoxide is found increasing towards the center of the particle. Hydrogen is uniform at

TABLE 1. CHAR DATA AND PHYSICAL PROPERTIES

$\rho_0 = 340$ kg/m^3
$S = 424 \times 10^3$ m^2/kg
$\epsilon = 76.5\%$
$\gamma = 5.5$
$\nu = 0.75$
$W_b = 80\%$
$C_{ps} = 12.56$ kJ/kgmole-°K
$\mathscr{D} = 2 \times 10^{-6}$ m^2/s
$h = 6.753.10^{-5}/R_c$ (kJ/m^2-s-°K)
$-\Delta H_1 = -131\,386.0$ (kJ/kmole)
$-\Delta H_2 = -170\,114.0$ (kJ/kmole)
$-\Delta H_3 = 7\,4897.7$ (kJ/mole)
$-\Delta H_4 = 41\,189.7$ (kJ/kmole)
$h_1^\circ = -241\,984.5$ (kJ/kmole)
$h_2^\circ = 0.0$ (kJ/kmole)
$h_3^\circ = -110\,603.0$ (kJ/kmole)
$h_4^\circ = -393\,777.0$ (kJ/kmole)
$h_5^\circ = -74\,897.7$ (kJ/kmole)

Sensible enthalpy data from von Fredersdroff and Elliott (1963).

the ambient value owing to the assumption with respect to its diffusion coefficient. The increase in methane molefraction towards the center is negligible. Hydrogen and methane profiles are omitted in many figures as no notable changes were observed with respect to the parameters studied. The carbon dioxide profiles show some unusual behavior. Carbon dioxide, a reactant in reaction 2, can be a product in reaction 4, and the behavior observed is the result of the competitive interaction between the two reactions. We notice a maximum in the profile (Figure 1*c*), indicating the crossover of the domination of these two reactions.

At $Sh = 2.0$ (that is, low mass transfer coefficient or large film thickness, $b \sim 4.5$), there is a significant drop in concentrations in the film (Figures 1*a* and *b*). The boundary layer thickness decreases with increasing mobility of the particle, and at $Sh = 25.0$ ($b \sim 0.4$), the film resistance is substantially decreased (Figures 1*c* and *d*). With increase in temperature, the concentration profiles become steeper in all cases. At $Sh = 2.0$, there are significant gradients both in the boundary layer and within the particle, whereas at $Sh = 25.0$, the gradients within the particle are very prominent (Figures 1*c* and *d*). At 1 400°K (Figure 1*d*), the reaction zone is close to the surface of the particle. In all cases except Figure 1*b*, the profiles shown are for time $t = 0$ (that is, zero conversion). The development of the concentration profiles are shown in Figure 1*b*. As gasification proceeds, conversion level increases, rates drop the profiles become less steep and

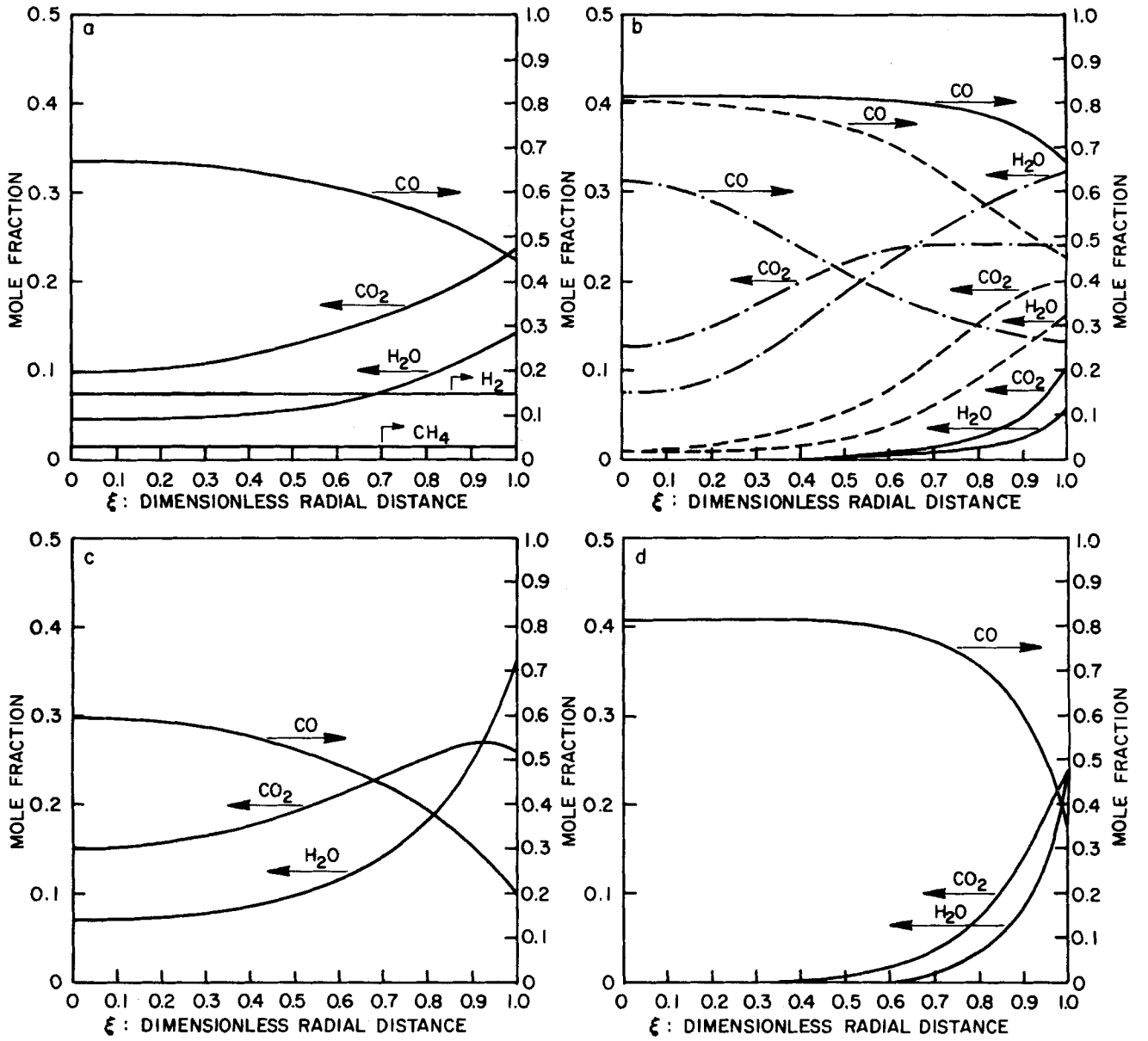

Figure 1. Concentration profiles at $x_{b1} = 50\%$, $x_{b2} = 15\%$, $x_{b5} = 3\%$, $P = 506.5$ kN/m^2, $R_c = 5 \times 10^{-4}$ m. *a*. $T_b = 1\,300$°K, $Sh = 2$ and $X = 0$. *b*. $T_b = 1\,400$°K, $Sh = 2$, ——— at $(t, X) = (0, 0)$, ----- $(t, X) = (27.1, 0.76)$ and —·—·— $(t, X) = (42.4, 0.98)$. *c*. $T_b = 1\,300$°K, $Sh = 25$ and $X = 0$. *d*. $T_b = 1\,400$°K, $Sh = 25$ and $X = 0$.

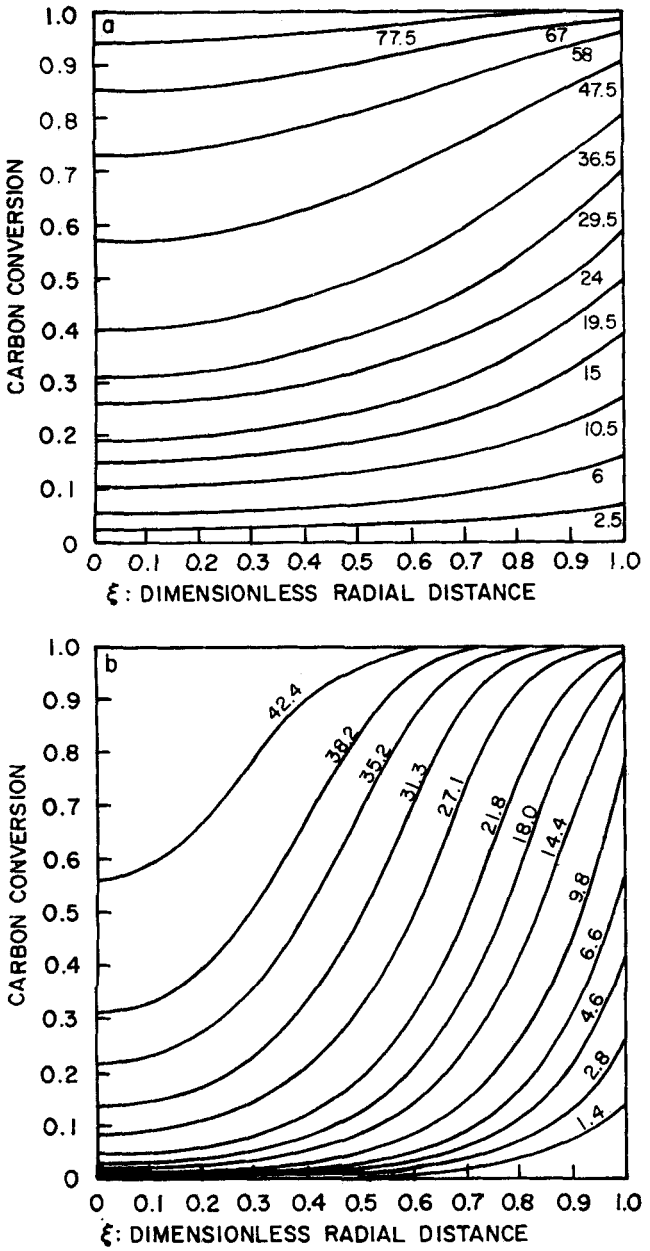

Figure 2. Conversion profiles at various time (s) for x_{b1} = 50%, x_{b5} = 3%, Sh = 2, R_c = 5 × 10^{-4} m, P = 506.5 kN/m². *a*. T_b = 1 300°K. *b*. T_b = 1 400°K.

eventually tend to uniform ambient conditions at complete conversion. Note that the overall effect is consumption of carbon dioxide during the initial stages of gasification.

In most mathematical studies of gasification systems, uniform conversion within the char particle is assumed at all stages of gasification. In some cases, such assumptions have been used in determining reaction rates and kinetic parameters. Uniform conversion is a consequence of uniform reaction within the particle. This is true at low temperatures. As reaction proceeds, owing to the difference in reaction rates within the particle, a conversion profile develops, Figures 2*a* and *b*. From an initial conversion of zero, the profile becomes steeper with reaction, and at high conversions the profiles become less steep and eventually tend to the value 1 everywhere. At temperatures less than 1 150°K, the profiles are almost flat, but as temperature increases, the profiles become very steep (Figures 2*a* and *b*). The development of the concentration profiles in Figure 1*b* corresponds to the development of the conversion profiles in Figure 2*b*. Further, in Figure 2*b* note that the core size starts to shrink after a certain time and will have a definite size when the particle nears complete conversion. One concludes that neither the shrinking core model nor the homogeneous model is applicable in this case. With higher char reactivities and higher temperature, one can expect the particle to react more like a shrinking core.

The behavior of the system for various total pressures is shown in Figures 3*a*, *b* and *c*. In Figure 3*a*, we notice that in the initial stages the curves are linear, implying not much change in total gasification rate. At higher conversions, as the rates diminish, there is a rapid increase in gasification time. An increase in pressure from 101.3 to 506.5 kN/m² has a substantially greater influence than an increase from 506.5 to 3 039 (kN/m²). If the amount of carbon was the only factor on which the gasification rate depended, the gasification rate curves (Figure 3*b*) would be straight lines going to zero at conversion one. But the behavior observed is to a great extent caused by the changes in the internal structure. Carbon depletion and the initial increase in surface area have compensating effects on the gasification rate which is observed as the flattening of the curves. At low pressures, there is a sharp decrease in the gasification time accompanied by an increase in effectiveness factor (Figure 3*c*), and the variation decreases at high pressure. Therefore, little is gained by increasing the pressure above a certain level.

The influence of the surface area changes are clearly seen in the effectiveness factor curves (Figure 4). The fact that EF2, based on the initial surface area of the particle, is greater than one implies that the influence of the increase in surface area is so great that it is even higher than the diffusional effects. The initial drop in EF and EF2 is due to the temperature drop in the particle, providing heat for the endothermic reactions. It is found that the temperature difference between the particle and the bulk is no greater than 5°K. Hence, the particle can be assumed to be at the ambient temperature.

Effectiveness factors and the time for 95% conversion delineate the effects of ambient temperature on the system (Figure 5). At low temperatures, there is practically no reaction, and EF is almost one, while at higher temperatures, EF drops sharply. At low Sh numbers most resistance is offered by the gas film, but when Sh is increased, the profiles in the particle become steep (the gas film resistance is low), and this should shift the curve to the right, as shown for Sh = 2.0 and Sh = 25.0. Though it is not apparent, the EF in the temperature range 900° to 950°K is found to be slightly greater than one. The nonlinear interaction of the water-gas shift equilibrium demands a higher concentration of carbon dioxide, and thus the CO_2 concentration is greater than the bulk value. This can compensate the decrease in steam gasification rate and be in excess. The time for 95% conversion is seen to decrease sharply and then level off; the decrease is due to increased rates of gasification, and the leveling off is caused by the decline in EF.

Depending on whether reaction 2 or 4 is dominating, carbon dioxide can be a reactant or a product. This depends strongly on the other reactions taking place and on the ambient conditions. The behavior is seen in Figure 5. At lower temperatures (900° to 1 200°K), the carbon dioxide gasification rates are low (10^{-5} to 10^{-1} kgmole/m³−s) and the shift equilibrium constants are high (4 to 1). Hence, carbon dioxide is produced. As the temperature increases, the situation reverses, and the carbon dioxide flux declines. At a certain point, carbon dioxide is neither produced nor consumed. Further increase in temperature results in carbon dioxide consumption.

Concentration of steam in the bulk is found to have a significant effect on the gasification rate (Figure 6). The gasification rate increases with steam molefraction, and, accordingly, the time for gasification decreases. The increase in overall rates is not proportional to the increase in ambient steam molefraction, and hence EF decreases. However, operation under high steam molefraction should be advantageous owing to higher rates. The amount of hydrogen in the bulk also plays an important role (Figure 7). The change in hydrogasification rate due to variations in hydrogen concentration has negligible overall effect because these rates are very low. But hydrogen has a powerful retarding effect on steam gasification. Hence, the total rate decreases and

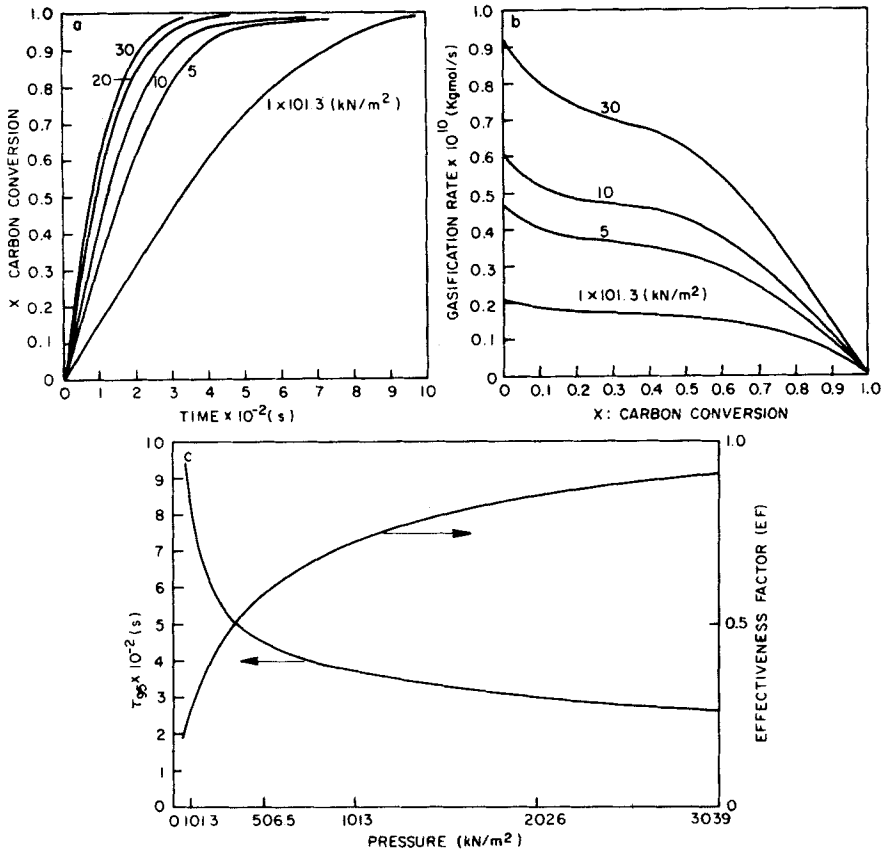

Figure 3. Effect of pressure on, a. gasification time, b. gasification rate and c. effectiveness factor and τ_{95} at T_b = 1 200°K, x_{b1} = 50%, x_{b2} = 15%, x_{b5} = 3%, R_c = 5 × 10^{-4} m and Sh = 2.

time for 95% conversion increases. The decrease in reaction rates is not proportional to the increase in hydrogen concentration because hydrogasification rate increases and the surface concentration of water increases as the shift equilibrium demands a higher concentration, and hence EF increases.

In a fluidized bed reactor, the particle size ranges up to 5 mm (Rudolph, 1976), and in moving bed reactors the average particle size is higher. It is, therefore, important to study the influence of particle size. The drop in EF with increase in particle size is quite steep (Figure 8). At high Sh, the intraparticle diffusion is predominant, and, again, EF drops. We conclude that the diffusional effects are significant and become acute with increase in particle size. Sherwood number has a strong effect in the range 2 to 30 (Figure 9). Above ~100, the resistance of the film is almost negligible.

At this stage our aim is to compare the present model with some existing empirical relations. Johnson (1974) presented a set of gasification kinetics for bituminous coal char, in particular Pittsburgh HVab char, and Gibson-Euker (1975) present results

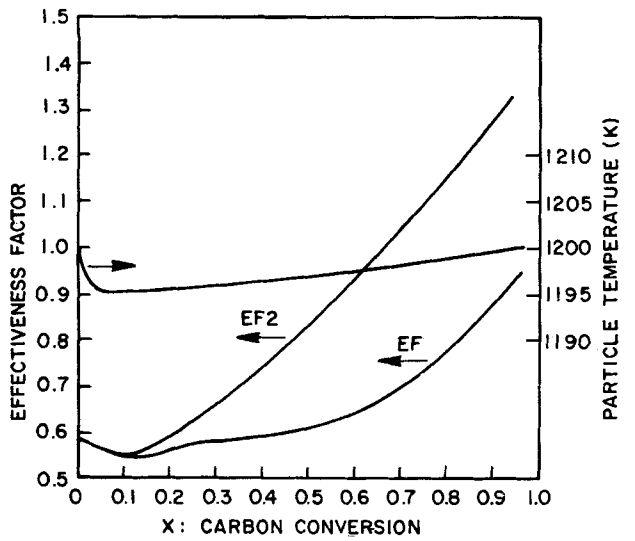

Figure 4. Effectiveness factors EF and EF2 and particle temperature with average conversion at x_{b1} = 50%, x_{b2} = 15%, x_{b5} = 3%, T_b = 1 200°K, R_c = 5 × 10^{-4} m, P = 506.5 kN/m^2 and Sh = 2.

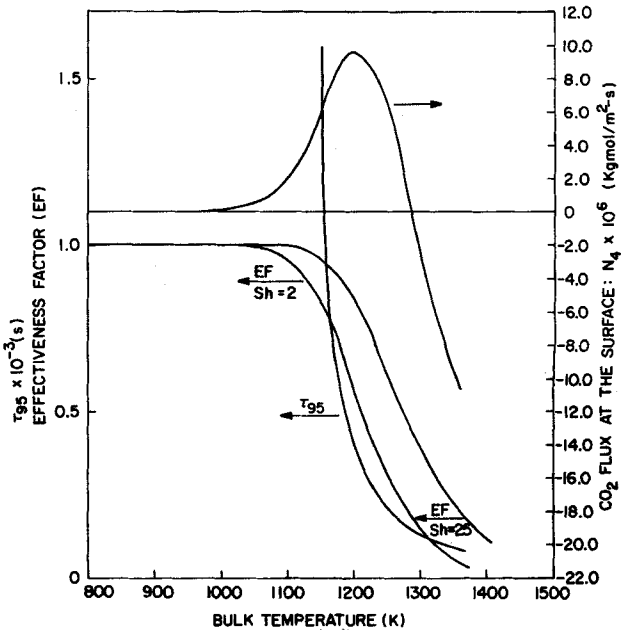

Figure 5. Effect of bulk temperature at P = 506.5 kN/m^2, x_{b1} = 50%, x_{b2} = 15%, x_{b5} = 3% and R_c = 5 × 10^{-4} m. τ_{95} at Sh = 2, N_4 at Sh = 2 and X = 0 and EF at X = 0.

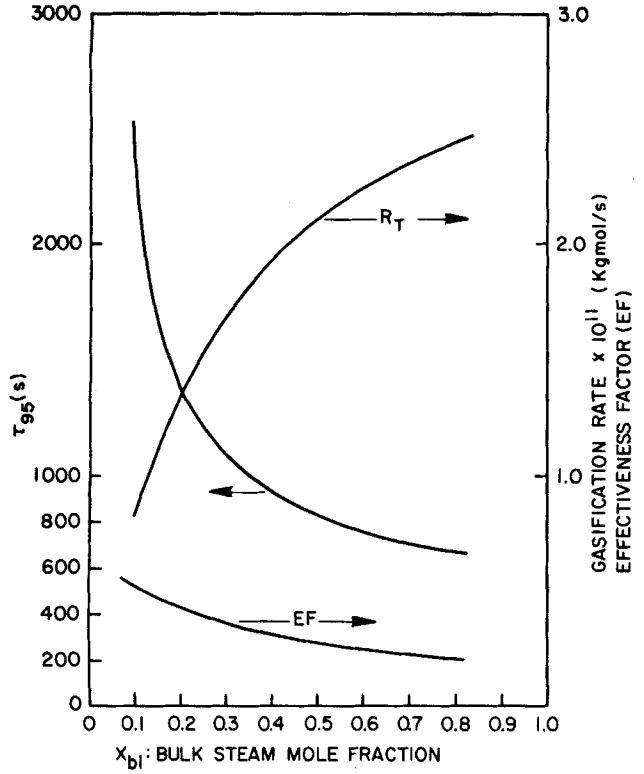

Figure 6. Effect of bulk steam concentration at T_b = 1 200°K, P = 101.3 kN/m², x_{b2} = 15%, x_{b5} = 3%, $R_c = 5 \times 10^{-4}$ m and Sh = 2. R_T, x_{1s} and EF at X = 0.

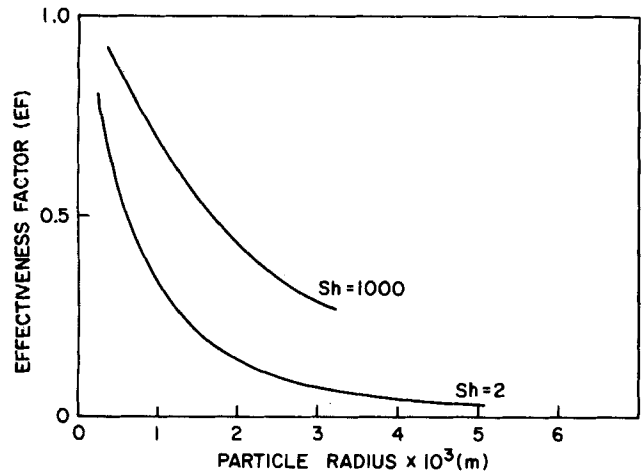

Figure 8. Influence of particle size on effectiveness factor at T_b = 1 200°K, P = 506.5 kN/m², x_{b1} = 50%, x_{b2} = 15%, x_{b5} = 3% and X = 0.

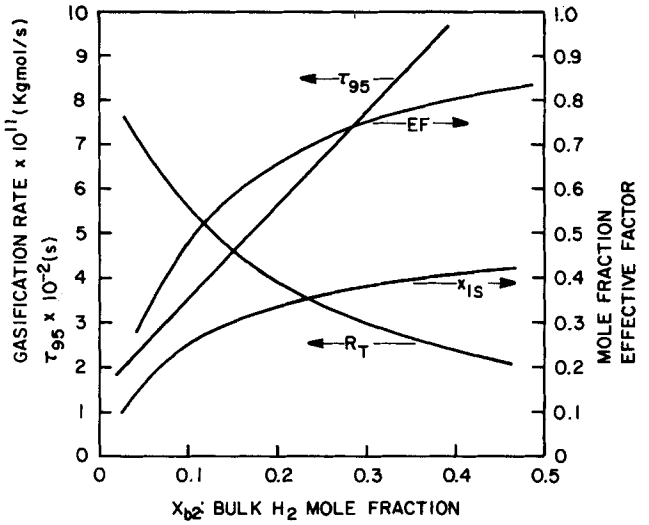

Figure 7. Effect of bulk hydrogen concentration at T_b = 1 200°K, x_{b1} = 50%, x_{b5} = 3%, P = 506.5 kN/m², $R_c = 5 \times 10^{-4}$ m and Sh = 2. R_T, x_{1s} and EF at X = 0.

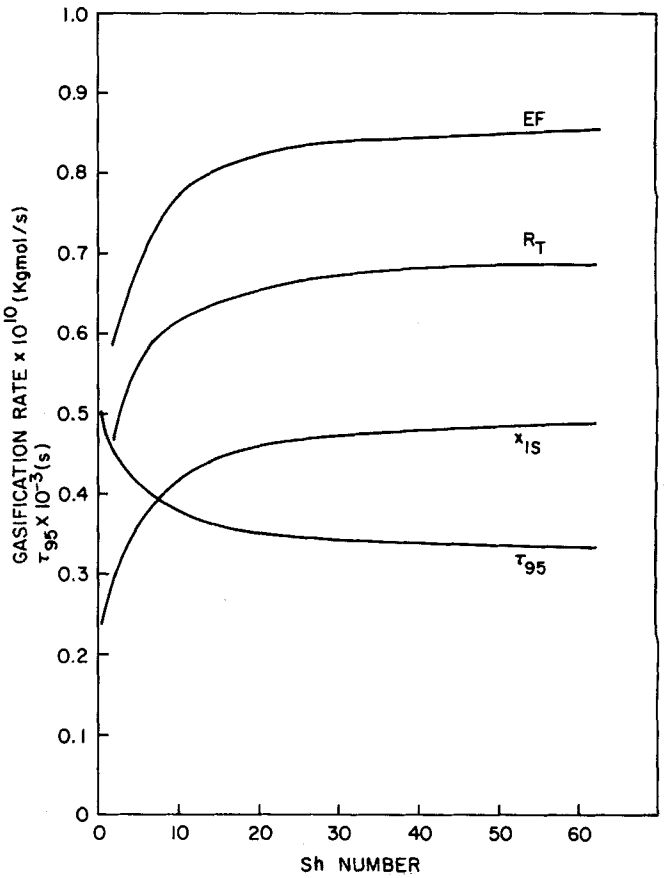

Figure 9. Effect of Sh number at T_b = 1 200°K, x_{b1} = 50%, x_{b2} = 15%, x_{b5} = 3%, P = 506.5 kN/m², EF, R_T and x_{1s} at X = 0.

for Illinois and Wyoming coal char. Bituminous coal char has surface area in the range 10 to 15 $\times 10^3$ m²/kg (Dutta et al., 1977) which is low compared to the value we have been using. An appropriate set of physical properties is chosen for HVab char, and further it is assumed that the char lost surface area with gasification and relative available surface area a is chosen accordingly. Since there are no data available on the available surface area, a can be treated as a parameter. Figures 10*a*, *b* and *c* show comparisons at different particle sizes. For small particles (Figure 10*a*), when diffusional effects are not significant, the model agrees well with the relations presented by Johnson. Further, computations of the present model with no change in surface area with gasification shows that the char used in Johnson's work lost surface area with gasification. The G-E kinetics, however, shows no variation other than the first-order dependence on the amount of carbon, which indicates that the change in surface area was probably not considered. As the particle size increases (Figures 10*b* and *c*) the difference between the model and the empirical relation increases. The present model predicts lower rates because of diffusional effects. The time-conversion plot (Figure 10*d*) shows that the empirical relation is independent of particle size. The present model, however, shows a strong dependence, and larger particles take a longer time to attain the same conversion levels. Hence, this empirical relation may not predict the gasification behavior when diffusional effects are important, and it is applicable only to a particular type of char. If the physical properties of the coal/char are known, the present model should predict gasification behavior under somewhat broader conditions.

So far in our calculations we have neglected the convective terms in the equations. On inclusion of the convective terms,

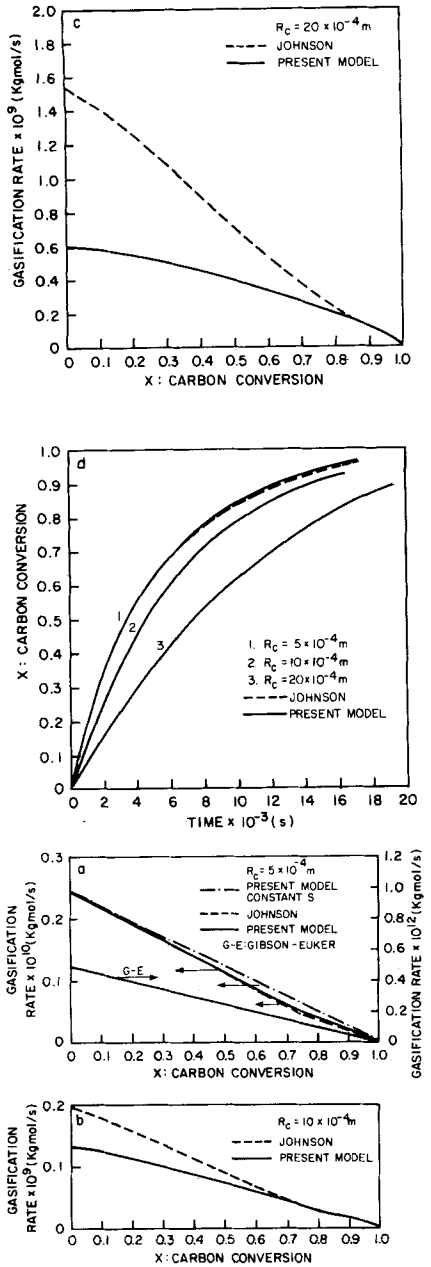

Figure 10. Comparisons with Johnson's relation for bituminous coal char at $T_b = 1\,300°K$, $x_{b1} = 50\%$, $x_{b2} = 15\%$, $x_{b5} = 3\%$, $P = 506.5$ kN/m^2, $Sh = 2$, $S = 12 \times 10^3$ m^2/kg, $\rho_0 = 340$ kg/m^3, $\nu = 0.8$, $\gamma = 6.0$ and $W_b = 0.8$.

note that a factor $(1 + z)$ appears in the differential equation. Since z is positive, this factor should induce additional resistance to diffusion. The concentration profile obtained for the Stefan flow problem are slightly steeper than that of the non-Stefan flow problem, and consequently one has lower effectiveness factor and overall gasification rate. There is no difference in behavior of the two systems. The magnitude of the difference is less than 3%. Hence, the convective terms may be neglected.

ACKNOWLEDGMENT

The authors are indebted to the Robert A. Welch Foundation for financial support of this work.

NOTATION

a = relative available surface area
A = external surface area of the particle, m^2
b = ratio of boundary layer thickness to the radius of the particle
C = total concentration, kgmole/m^3
C_i = concentration of the i^{th} species kgmole/m^3
C_{pi} = specific heat of i^{th} species, kJ/kgmole-°K
C_{ps} = specific heat of the solid, kJ/kgmole-°K
$\mathscr{D}$ = binary diffusion coefficient, m^2/s
$\mathscr{D}_{ik}$ = gas binary diffusion coefficient of the i-k^{th} pair, m^2/s
D = effective diffusivity, m^2/s
EF, EF2 = effectiveness factor as defined in Equations (20a) and (20b), respectively
h = heat transfer coefficient, kJ/m^2-s-°K
h_i = molar enthalpy of the i^{th} species, kJ/kgmole
h_i° = heat of formation of the i^{th} species at reference temperature, kJ/kmole
(k_1, k_{12}), k_2 and k_3 = rate constants appearing in reactions 1, 2 and 3, respectively
k_g = mass transfer coefficient, m/s
K = equilibrium constant of the shift reaction
M = mass of the particle, kg
M_0 = original mass of the particle, kg
N_i = flux of the i^{th} species, kgmole/m^2-s
P = total pressure, N/m^2
p_{H_2} = partial pressure of hydrogen, N/m^2
r = radial coordinate, m
r_j = specific rate of the j^{th} reaction per unit volume of the particle, kgmole/m^3-s
rs_j = specific rate of j^{th} reaction per unit internal area, kgmole/m^2-s
R = universal gas constant, kJ/kgmole-°K
R_c = radius of the particle, m
R_T = total gasification rate, kgmole/s
S = original specific surface area of the particle, m^2/kg
Sh = Sherwood number, $2.R_c\, k_g/D$
t = time, s
T = temperature, °K
T_b = bulk temperature, °K
T_p = particle temperature, °K
V = volume, m^3
V_p = volume of the particle, m^3
$\overline{w}$ = defined as in Equation 25
W_b = original carbon content in the particle
X = average carbon conversion of the particle
X_r = carbon conversion at position r in the particle
x_i = molefraction of i^{th} species
x_{bi} = molefraction of i^{th} species in the bulk
y_i = defined in Equation (24)
z, z_b = defined in Equation (15c)

Greek Letters

α_{ij} = stoichiometric coefficient, i^{th} species, i^{th} reaction
β = as defined in Equation (15c)
γ = parameter in Equation (1)
ΔH_j = heat of j^{th} reaction, kJ/kgmole
Δt = time interval, s
ΔT = temperature difference, °K
ϵ = porosity of the particle
ν = parameter in Equation (1)
ξ = dimensionless radial coordinate, r/R_c
ρ = density of the particle, kg/m^3
ρ_0 = original density of the particle, kg/m^3
τ_{95} = time for 95% conversion, s

Subscripts

i = i^{th} gaseous species, 1:H_2O, 2:H_2, 3:CO, 4:CO_2, 5:CH_4
j = j^{th} reaction, 1, 2, 3 and 4
k = k^{th} gaseous species, 1, 2, 3, 4 and 5
s = condition at the particle surface

Superscript

$*$ = dimensionless quantity

LITERATURE CITED

Badzioch, S., D. R. Gregory, and M. A. Field, "Investigation of the Temperature Variation of the Thermal Conductivity and Thermal Diffusivity of Coal," *Fuel*, **43**, 267 (1964).

Blackwood, J. D., "The Reaction of Carbon with Hydrogen at High Pressure," *Australian J. Chem.*, **12**, 14 (1959).

Caram, S. H., and N. R. Amundson, "Fluidized Bed Gasification Reactor Modelling 1. Model Description and Numerical Results of a Single Bed," *Ind. Eng. Chem. Process Design Develop.*, **18**, 80 (1979).

Dutta, S., C. Y. Wen, and R. J. Belt, "Reactivity of Coal and Char. 1. In Carbon Dioxide Atmosphere," *ibid.*, **16**, 20 (1977).

Field, M. A., D. W. Gill, B. B. Morgan, and P. G. W. Hawksley, "Combustion of Pulverized Coal," BCURA Leatherhead, Cherey and Sons Ltd., Banbury, England (1967).

Gibson, M. A., and C. A. Euker, Jr., "Mathematical Modeling of Fluidized Bed Gasification," Paper presented at the 68th AIChE Annual Meeting, Los Angeles, Calif. (1975).

Hashimato, K., and P. L. Silveston, "Gasification: I. Isothermal, Kinetic Control Model for Solid with Pore Size Distribution," *AIChE J.*, **19**, 259 (1973*a*).

Hashimato, K., and P. L. Silveston, "Gasification: II. Extension to Diffusion Control," *ibid.*, **19**, 268 (1973*b*).

Hedden, K., and A. Lowe, "Über die vergasung von reactographit mit kohlendioxid und wasserdampf," *Carbon*, **5**, 339 (1967).

Johnson, J. L., "Kinetics of Bituminous Coal Char Gasification with Gases Containing Steam and Hydrogen," *Adv. Chem. Ser.*, No. 131, 145 (1974).

Kawahata, M., and P. L. Walker, Jr., "Mode of Porosity Development in Activated Anthracite," *Proc. 5th Carbon Conf.*, **11**, 251 (1963).

Mulcahy, M. F. R., and I. W. Smith, "Kinetics of Combustion of Pulverized Fuel: A Review of Theory and Experiments," *Rev. Pure Appl. Chem.*, **19**, 81 (1969).

Petersen, E. E., P. L. Walker, Jr., and C. C. Wright, "Surface Area Development Within Artificial Graphite Rods Reacted with Carbon Dioxide Form 900° to 1300°C," *Ind. Eng. Chem.*, **47**, 1629 (1955).

Rudolph, P. F. H., "Art of Coal Gasification," *Chem. Reac. Eng. Proc., 4th Int/6th Eur. Sym.*, Heidelberg, Fed. Rep. Ger. (Apr. 6-8, 1976).

Turkdogan, E. T., R. G. Olsson, and J. V. Vinters, "Pore Characteristics of Carbons," *Carbon*, **8**, 545 (1970).

Villadsen, J., and M. L. Michelsen, *Solution of Differential Equation Models by Polynomial Approximation*," Prentice-Hall, Englewood Cliffs, N.J. (1978).

Von Fredersdroff, C. G., and M. A. Elliott, "Coal Gasification," in *Chemistry of Coal Utilization*, H. H. Lowry, ed., p. 892, Supl. vol., J. Wiley, New York (1963).

Walker, P. L., Jr., R. J. Foresti, Jr., and C. C. Wright, "Surface Area Studies of Carbon—Carbon Dioxide Reaction," *Ind. Eng. Chem.*, **45**, 1703 (1953).

Walker, P. L., F. Rusinko, and L. G. Austin, "Gas Reactions of Carbon," *Adv. Catal.*, **11**, 134 (1959).

Yang, R. T., and M. Steinberg, "A Diffusion Cell Method for Studying Heterogeneous Kinetics in the Chemical Reaction/Diffusion Controlled Regime. Kinetics of C + $CO_2 \rightarrow 2CO$ at 1200-1600°C," *Ind. Eng. Chem. Fundamentals*, **16**, 235 (1977).

Manuscript received June 5, 1979; revision received October 12, and accepted October 24, 1979.

Identification and Linear Multivariable Control in an Absorption-Desorption Pilot Plant

A study of the identification of the dynamics of a pilot scale absorption-desorption system and the subsequent design of a multivariable control scheme are reported. A multivariable transfer function model was obtained from experimental input-output data in which the inputs (steam supply and liquid circulation rate) were perturbed simultaneously using uncorrelated pseudo random sequences. A two-step, least-squares estimator was employed for the identification of the model.

A multivariable controller was then designed on the basis of the direct Nyquist array method. The implementation of the controller design indicated the utility of the design procedure as compared to independent single input, single output control loops; there is, however, some scope for additional tuning.

J. J. ALBRECHT

L. S. KERSHENBAUM

and

D. L. PYLE

Department of Chemical Engineering and Chemical Technology
Imperial College
London SW7, England

SCOPE

In recent years, several applications of modern control theory have been proposed for use in the chemical industry. However, despite the obvious theoretical advantages of these advanced strategies, their implementation in an on-line situation generally requires excessive computational effort. An alternative approach is the extension of well-proven frequency domain design methods to multivariable cases; this offers the advantages of easy implementation and the possibility of on-line adjustment or tuning of the controller. The design proceeds in two stages: a simple model of the system is first obtained, and a controller is then designed based on that model. In the linear case, it is possible to deduce from experimental input/output measurements a process model which represents the best linear fit of the nonlinear chemical process. It has been shown that the use of pseudo random binary sequences (PRBS) as input disturbances offers significant advantages over other forms of input signals such as square wave or sinusoidal excitation.

The multivariable controller can then be designed using one of several extensions of the Nyquist criterion to multivariable systems (Rosenbrock, 1974). Although

Correspondence concerning this paper should be addressed to L.S. Kershenbaum.-J.J. Albrecht is with Lurgi Kohl und Mineralöltechnik, Frankfurt, Germany.